



GRASIAN: towards the first demonstration of gravitational quantum states of atoms with a cryogenic hydrogen beam

Carina Killian^{1,a} , Zakary Burkley^{2,b}, Philipp Blumer^{2,c}, Paolo Crivelli^{2,d}, Fredrik P. Gustafsson^{1,e}, Otto Hanski^{3,f}, Amit Nanda^{1,g}, François Nez^{4,h}, Valery Nesvizhevsky^{5,i}, Serge Reynaud^{4,j}, Katharina Schreiner^{2,5,k}, Martin Simon^{1,l}, Sergej Vasiliev^{3,m}, Eberhard Widmann^{1,n}, and Pauline Yzombard^{4,o}

¹ Stefan Meyer Institute for Subatomic Physics, Austrian Academy of Sciences, Kegelgasse 27, 1030 Vienna, Austria

² Institute for Particle Physics and Astrophysics, ETH, Zurich, 8093 Zurich, Switzerland

³ Department of Physics and Astronomy, University of Turku, 20014 Turku, Finland

⁴ Laboratoire Kastler Brossel, Sorbonne Université, CNRS, ENS-PSL Université, Collège de France, 75252 Paris, France

⁵ Institut Max von Laue - Paul Langevin, 71 avenue des Martyrs, 38042 Grenoble, France

Received 2 February 2023 / Accepted 12 March 2023 / Published online 29 March 2023

© The Author(s) 2023

Abstract. At very low energies, a light neutral particle above a horizontal surface can experience quantum reflection. The quantum reflection holds the particle against gravity and leads to gravitational quantum states (GQS). So far, GQS were only observed with neutrons as pioneered by Nesvizhevsky and his collaborators at ILL. However, the existence of GQS is predicted also for atoms. The GRASIAN collaboration pursues the first observation and studies of GQS of atomic hydrogen. We propose to use atoms in order to exploit the fact that orders of magnitude larger fluxes compared to those of neutrons are available. Moreover, recently the *q*-BOUNCE collaboration, performing GQS spectroscopy with neutrons, reported a discrepancy between theoretical calculations and experiment which deserves further investigations. For this purpose, we set up a cryogenic hydrogen beam at 6 K. We report on our preliminary results, characterizing the hydrogen beam with pulsed laser ionization diagnostics at 243 nm.

1 Introduction

Quantum bouncers were first predicted in 1928 [1]. Nearly 75 years later, this phenomenon was demonstrated through the observation of neutron (*n*) gravitational quantum states (GQS) [2–8]. Confined by the gravitational- and the mirror potential, the *n* are settled in gravitationally bound quantum states.

Studies of *n* GQS have a broad impact on fundamental and applied physics. They serve as a unique method to study the interaction of a particle in a quantum state with a gravitational field. For example, paired with more recent measurements of *n* whispering gallery states (WGS) - quantum states trapped by the centrifugal- and the mirror potential [9], they result in the first direct demonstration of the validity of the weak equivalence principle for a particle in a pure quantum state.

The observation of GQS initiated active analysis of the peculiarities of this phenomenon [10–17] and their application to the search for new physics, such as the searches for extra fundamental short-range interactions [18–24], verification of the weak equivalence principle in the quantum regime [25–27], extensions of quantum

Precision Physics of Simple Atomic Systems.

Guest editors: Paolo Crivelli, Krzysztof Pachucki, Wim Ubachs, Thomas Udem, and Stefan Ulmer.

^a e-mail: Carina.Killian@oeaw.ac.at (corresponding author)

^b e-mail: zakburkley@gmail.com

^c e-mail: Philipp.Blumer@cern.ch

^d e-mail: Paolo.Crivelli@cern.ch

^e e-mail: fredrik.parnefjord.gustafsson@cern.ch

^f e-mail: otto.o.hanski@utu.fi

^g e-mail: Amit.Nanda@oeaw.ac.at

^h e-mail: francois.nez@lkb.upmc.fr

ⁱ e-mail: nesvizh@ill.fr

^j e-mail: serge.reynaud@lkb.upmc.fr

^k e-mail: schreink@student.ethz.ch

^l e-mail: Martin.Simon@oeaw.ac.at

^m e-mail: servas@utu.fi

ⁿ e-mail: Eberhard.Widmann@oeaw.ac.at

^o e-mail: pauline.yzombard@lkb.upmc.fr

mechanics [28, 29], extensions of gravity and space theories [30–33] or tests of Lorentz invariance [34–36].

New fundamental short-range interactions are predicted in extensions of the Standard Model such as grand unified, supersymmetric and string theories that could alter the weak gravitational potential. They also appear in certain models explaining dark matter and dark energy [23]. Additionally, studies on GQS can provide extremely sensitive measurements of the mirror's surface potential and shape, which is of high interest to the surface physics community.

Spectroscopy and interferometry methods of observation of GQS of n have been analyzed theoretically and implemented experimentally over the previous two decades [37–41]. However, the existence of GQS is predicted also for atoms and antiatoms [42–50]. Those are expected to have essentially identical properties for particles of almost equal mass such as n , atomic hydrogen (H) or even antihydrogen (\bar{H}).

A major constraint to improve the precision of the current measurements of GQS of n is the limited density of ultracold n (UCNs). It looks natural to exploit the much higher fluxes available for atoms, namely the high densities of existing H -beams [51]. However, all the projects concerning the use and study of GQS of atoms are currently based only on theoretical estimations since those, in contrast to n , have never been observed experimentally. Only a direct experiment can prove the existence of GQS of atoms, evaluate the systematic and statistical uncertainties of such experiments and develop the experimental techniques needed for more precise measurements in the future.

In Sect. 2, a theoretical derivation of GQS is given. The method used earlier for the observation of n GQS and the planned implementation of a measurement with H is presented in Sect. 3. A detailed description of the GRASIAN experimental setup and the recent measurements is given in Sect. 4.

2 Theoretical framework

A sufficiently slow particle trapped by the gravitational field on one side and a horizontal reflective surface (“mirror”) on the other side settles in GQS. The particle's wave function $\psi(z)$ in the Earth's gravitational field above a mirror is governed by the Schrodinger equation $\frac{\hbar^2}{2m} \frac{d^2\psi(z)}{dz^2} + (E - mgz)\psi(z) = 0$, where \hbar is the reduced Planck constant, m is the particles mass, z is the height, E is the energy of the vertical motion of the particle, and g is the acceleration in the Earth's gravitational field. The only constant related to the particle's identity is it's mass, which is nearly exactly the same for n , H or \bar{H} . For simplicity, n over an ideal mirror will be considered in the following derivation.

An ideal horizontal mirror at the height $z = 0$ can be approximated as an infinitely high and abrupt potential step. This approximation is justified by the characteristic values of energies and lengths in our problem. The

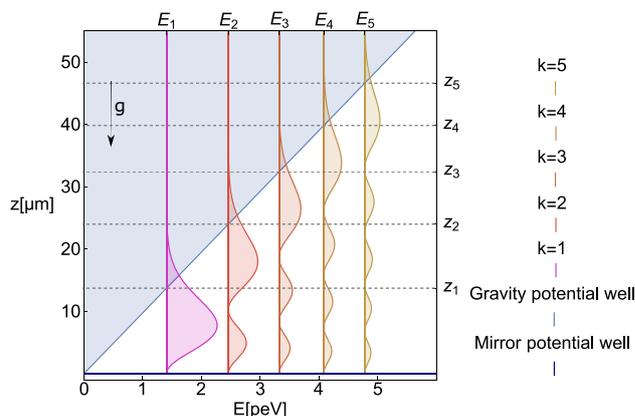


Fig. 1 Squared modules of the neutron wavefunctions $|\psi_k(z)|^2$ as a function of the height z for the five lowest quantum states; they correspond to the probabilities of observing neutrons at a height z

energy of neutrons in low quantum states $\sim 10^{-12}$ eV, is much smaller than the optical potential of the mirror material $\sim 10^{-7}$ eV [52], and the characteristic range of increase in the optical potential for a polished mirror $\sim 10^{-9}$ m, is much smaller than the wavelength of neutrons in low quantum states $\sim 10^{-5}$ m. Such an infinitely high and abrupt optical potential corresponds to the zero boundary condition for the wave function, $\psi(z = 0) = 0$.

A solution of the Schrodinger equation can be written in terms of the Airy function Ai , $\psi(z) = C\text{Ai}(z/z_0)$, where $z_0 = [\hbar^2/(2m^2g)]^{1/3} = 5.87\mu\text{m}$ is the characteristic length scale of the problem and C is a normalization constant. The Airy function zeros λ_k define the quantum state energies $E_k = mgz_0\lambda_k$, where $\varepsilon_0 = mgz_0 = 0.602\text{peV}$ is the characteristic energy of the problem and $f_0 = \varepsilon_0/(2\pi\hbar) = 145\text{Hz}$ is its characteristic frequency.

The five lowest zeros of the Airy function Ai are $\lambda_k = \{2.34, 4.09, 5.52, 6.79, 7.94\dots\}$. The eigenfunctions of the quantum states are $\psi_k(\xi(z)) \sim C_k\text{Ai}(\xi_k(z))$, where $\xi_k(z) = z/z_0 - \lambda_k$, and C_k are normalization constants.

The energy eigenvalues E_k depend only on m , g and \hbar , and are independent of the ideal mirror properties. Within the classical description, a neutron with the energy E_k can rise in the gravitational field up to the height $z_k = E_k/mg$. In quantum mechanics, the probability of observing a neutron with the energy E_k in the k^{th} quantum state at a height z is equal to the squared modulus of its wave function (see Fig. 1).

3 Measurement method

3.1 GQS measurement with n

In this section, the methods developed for the first observation of GQS of n at ILL will be described. The

experimental installation is a one component gravitational UCN spectrometer with a high energy and spatial resolution [3]. The principle of its operation, illustrated in Fig. 2, is the measurement of the n flux through a slit between the mirror on bottom and the flat scatterer on top as a function of the slit height Δz which can be changed and precisely measured.

The scatterer surface is smooth on a large scale but rough on the μm scale. The roughness amplitude is about a few μm , and is comparable to the characteristic scale z_0 of the problem. The scatterer's surface reflects n which reach it non specularly, mixing the vertical and horizontal velocity components of the n . Because the n horizontal velocity components are much larger than their vertical velocity components, such mixing causes numerous collisions of the n with the scatterer, thus resulting in a prompt loss of those n .

The length of the bottom mirror is chosen based on the energy time uncertainty relation $\Delta\tau\Delta E \geq \hbar/2$. The observation of the k^{th} quantum state is possible if the difference between the Eigenenergies of state $k + 1$ and state k , $\Delta E_{k+1,k}$ is bigger than the width of the k^{th} quantum state, δE_k : $\Delta E_{k+1,k} > \delta E_k$. As the state number k increases, $\Delta E_{k+1,k} \sim k^{-1/3}$ decreases until the levels pass into the classical continuum. Evidently, measurements of low quantum states are easier and more convenient. δE_k is defined by the time of flight of n above the mirror. Therefore, the mirror length is determined by the time interval needed to observe a n in a GQS: $\Delta\tau \sim 0.5\text{ms}$. It follows, that the mirror length should be $L \sim 10\text{cm}$ for low states and for n velocities $v_{\text{hor}} \sim 5 - 10\text{m s}^{-1}$.

The vertical scale in the problem is defined by the relation between momentum p , velocity v and wavelength λ : $p = mv = \hbar/\lambda$ and the momentum position uncertainty relation $\Delta p\Delta z \geq \hbar/2$. The smaller the n vertical velocity component, the larger the n wavelength associated with this velocity component. But the classical height up to which a n can rise in the gravitational field cannot be smaller than the quantum mechanical uncertainty of its vertical coordinate, i.e., the n wavelength. This relation determines the lowest bound state of n in the Earth's gravitational field. The height uncertainty is then $\Delta z \sim z_0$, and the ver-

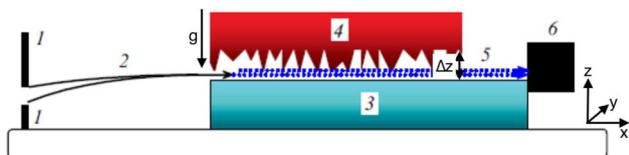


Fig. 2 Schematic of the experimental setup in the flow through mode. 1 are the bottom and top entrance collimator plates, arrows 2 correspond to neutron classical trajectories between the collimator and the entrance to the slit between mirror 3 and scatterer 4. Dotted horizontal arrows 5 illustrate neutron quantum motion above the mirror. 6 is the neutron detector. The height of the slit between the mirror and the scatterer can be varied and precisely measured

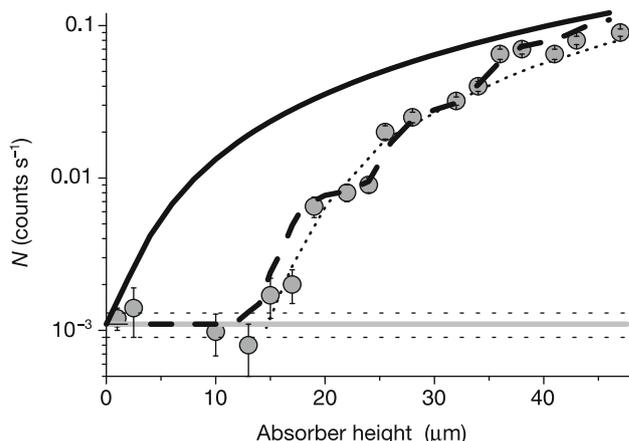


Fig. 3 The data points correspond to the measured n flux through the slit between mirror and absorber versus the slit width at low width values. The dashed curve is a fit using the quantum mechanical calculation, where all level populations and the height resolution are extracted from the experimental data. The solid curve is the full classical treatment. The dotted line is a truncated fit in which it is assumed that only the lowest quantum state - which leads to the first step - exists. Figure taken from [4]

tical velocity uncertainty is $\Delta v_z \sim v_0 = \sqrt{2\varepsilon_0/m} = 1.07\text{cm s}^{-1}$, the characteristic velocity in the problem.

The method used in the first observation of n GQS [4] consisted in measuring n transmission through the narrow slit Δz between the horizontal mirror and the scatterer above it. If $\Delta z \gg z_k$, neutrons in the k^{th} quantum state pass through the slit with no significant loss. But as Δz decreases, the neutron wave function $\psi_k(z)$ starts penetrating the scatterer, and the n loss probability increases. If $\Delta z \leq z_k$, the slit is practically nontransparent to neutrons in the k^{th} quantum state. In an "ideal" experiment with an infinitely high energy resolution, the n flux $N_{\text{QM}}(\Delta z)$ through the slit would sharply change at the height $\Delta z \sim z_k$. In reality, the idealized step like dependence is smoothed due to two factors: the spectrometer experimental resolution and the smooth shape of n wave functions. The latter is due to the tunneling of n through the gravitational barrier separating the classically allowed heights and the scatterer height. An example of the experimental data is shown in Fig. 3.

3.2 GQS measurement with H

The method, developed for the observation of GQS of n , will be used to demonstrate GQS of H . In the following section, the feasibility of such an experiment will be analyzed and the characteristic parameters of the two experiments will be compared.

The observation time is a key parameter. The time of observation is defined by the mean particle velocity and the mirror length. For the characteristic velocity of n , $v_n \sim 10\text{m s}^{-1}$ and the mirror length $L_n = 10\text{cm}$, the observation time was $\tau_n \sim 10\text{ms}$. $\tau_n/\tau_0 \sim 20$, i.e.,

the observation time is much larger than the formation time ($\tau_n \gg \tau_0$) and the GQS were well resolved. In order to provide the same conditions for the resolution of GQS, the time of observation of H has to be the same $\tau_H \sim \tau_n \sim 10\text{ms}$. For the planned GQS mirror length $L_H \sim 30\text{cm}$, the mean velocity of H has to be $v_H \sim L_H/10\text{ms} \sim 30\text{m s}^{-1}$. All H with significantly higher velocities do not settle in GQS, they only increase the background and have to be eliminated. Velocities of up to $v_H \sim 100\text{m s}^{-1}$ can still be tolerated, at the cost of a worse energy resolution of the experiment. This is still acceptable for the first observation of GQS of H . However, low velocities, good control over the velocity selection and sufficient background suppression is the key condition for the observation of GQS of H .

A major difference in the behavior of n and H , is the mechanism of their interaction with the rough surface of the scatterer. Scattered n are lost in the bulk of the mirror or scatterer after several reflections from their surfaces. Scattered H atoms have higher chances to leak through the slit and produce background. They escape from the slit into a broad angular distribution, in contrast to H , which pass the slit settled in a GQS. H atoms escaping to larger angles have to be eliminated to decrease the background. Therefore, it is very important to implement a proper background suppression.

The expected count rate of H is much higher than that of n . A simple comparison of the “brightness” of the n source at ILL and the H source at the GRASIAN experiment at ETH Zurich is the following. The total number of the particles produced at ILL is $\sim 10^{19}\text{s}^{-1}$, while it is $\sim 10^{17}\text{s}^{-1}$ at ETH. A characteristic temperature of n spectrum at ILL is $\sim 40\text{Kt}$, while it is $\sim 6\text{K}$ at ETH. An effective surface area of the source at ILL is $\sim 10^5\text{cm}^2$, while it is $\sim 1\text{cm}^2$ at ETH. These values result in a $\sim 10^4$ higher flux of particles at ETH. This estimation does not account for the velocity and spatial distributions of the particles at the two sources, the detection efficiencies, the transport losses, the experiment geometries etc. but gives a fair overall gain factor and the conclusion that H fluxes are much higher than those available at the best existing UCN sources. A more detailed calculation provides the same estimate of the count rate for this setup: $\sim 10^3 H\text{s}^{-1}$ for the lowest GQS, over four orders of magnitude larger than measured with n . With these increased count rates, and the minimal background with the H detection method based on the photoionization described in Sect. 4.1, one can measure the height distribution covering the first four GQS with a $1\mu\text{m}$ resolution and 5% accuracy in a matter of hours (compared to several days with the original n experiment). These robust statistics will give fast feedback, enabling us to solve experimental challenges quickly and efficiently.

4 Grasian cryogenic H -beam

In this section the GRASIAN cryogenic H -beam, located at ETH Zurich, will be described. It was originally devel-

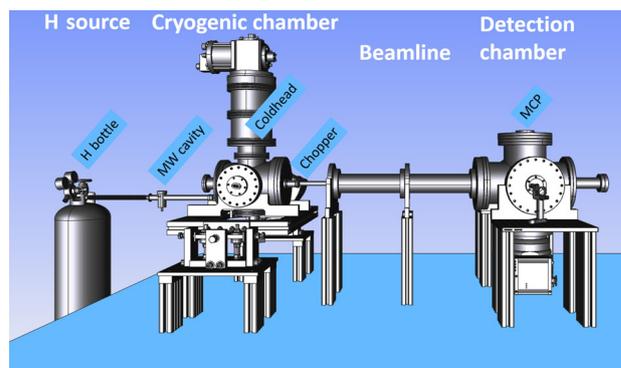


Fig. 4 Rendering of the ETH cryogenic H -beam setup

oped in the context of the ASACUSA [53], MuMASS [54,55] and GBAR [56] experiments to test and commission detectors, microwave- and laser-setups. It will be used for our attempt to demonstrate GQS of atoms for the first time.

The ETH H -beam consists of an H source, a cryogenic chamber, a beamline and a detection chamber. A schematic of the setup is shown in Fig. 4. The GQS chamber, which will contain the mirror-absorber system described in Sect. 3, will be installed in the near future.

In the H source, molecular hydrogen gas (H_2) is injected into a microwave cavity with a flow of $\sim 0.8\text{mL/min}$. Within the cavity, microwaves with 20–30W at 2400MHz, dissociate the H_2 into atomic H . The cracking efficiency was measured to be $\sim 80\%$, resulting in an H flux of more than 10^{17}atoms/s .

The generated atomic H is directed into the cryogenic chamber through a glass-TEFLON tube. The tube is inserted into a bent nozzle, directly connected with a coldhead to thermalize the atoms to $\sim 6\text{K}$ with minimal recombination. After the cryogenic chamber, the beam of atomic H is divided into bunches of $\sim 10^{14}\text{atoms/s}$ by a rotating chopper wheel. The H bunches flow through a system of velocity selecting apertures into the detection chamber at the end of the beamline.

A 243nm ultraviolet (UV) laser is directed into the detection chamber in a perpendicular direction with respect to the atomic beam and is retro reflected by a mirror on the other side. This setup creates two counter propagating beams, as required to excite the hydrogen atoms from the 1S to the 2S state via a two photon transition. A third photon from the same laser induces photoionization, the resulting protons can be detected by a microchannel plate (MCP).

4.1 The laser system for hydrogen detection

The H 1S-2S transition is dipole forbidden, hence it is only possible to drive it with two photons. The energy of this transition is split between the two photons involved, meaning that the wavelength of the laser driving this transition has to be $\sim 243\text{nm}$. As a dipole forbidden transition is very unlikely, a high photon den-

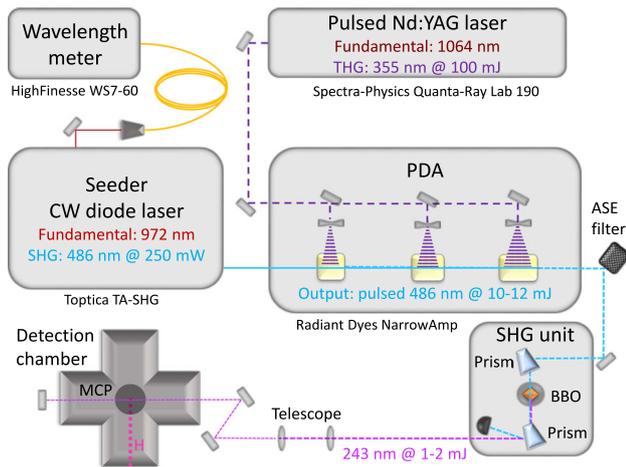


Fig. 5 Schematic of the laser system. The PDA is pumped with a pulsed Nd:YAG laser and seeded with a CW diode laser. The generated 486nm pulsed beam is frequency doubled in the SHG unit and afterward sent into the detection chamber to ionize H . The wavelength of the fundamental of the seeder laser, is determined and controlled by a wavelength meter

sity and hence a high intensity laser is needed for efficient excitation and subsequent ionization of H atoms. The most efficient realization is a pulsed laser. Such a laser system has been set up at ETH Zurich. It will be described in the following section.

A schematic of the laser system is shown in Fig. 5. It consists of two lasers - a continuous wave¹ (CW) and a pulsed laser,² a pulsed dye amplifier³ (PDA) and a second harmonic generation (SHG) unit. The fundamental of the CW laser has a wavelength of 972nm. An internal SHG cavity creates the output CW laser beam with a wavelength of 486nm and an average power of ~ 250 mW. With exactly double of the desired wavelength for the two photon 1S-2S transition, the CW laser acts as the seeder laser. The pulsed laser is the 355nm third harmonic of a 10 Hz pulsed Nd:YAG laser. In the Q-switch mode, the pulses are 10 ns long and have a pulse energy of ~ 100 mJ.

Within the PDA, three quartz cuvettes are circulated with the dye, Coumarin 102, dissolved in ethanol. The absorption and fluorescence of Coumarin 102 fit the application well: when pumped with 355 nm light, the emission is centered around 473 nm. The pulsed laser is split up and focused onto the three cuvettes, and pumps the Coumarin molecules. The CW beam seeds the PDA by passing through the three cuvettes overlapping with the pumped dye molecules. This stimulates the emission of 486nm photons with every pulse that pumps the dye. After three cuvettes, ~ 10 – 12 mJ of 486 nm pulsed laser light is generated. Like the pulsed pump laser, it runs at 10 Hz with a pulse length of ~ 10 ns.

¹ Toptica TA-SHG pro.

² Spectra-Physics Quanta-Ray Lab 190.

³ Radiant Dyes NarrowAmp.

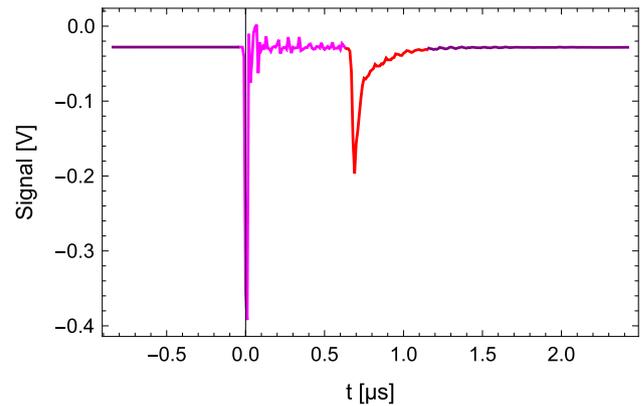


Fig. 6 Waveform captured by the oscilloscope showing the H^+ signal. The purple region determines the offset in the signal strength evaluation. The magenta curve corresponds to the signal induced by the UV light in the detection chamber. The red curve corresponds to the H^+ induced voltage change in the expected time-of-flight window between 640ns to 1.15 μ s

In the SHG unit, the output of the PDA is frequency doubled with a barium borate (BBO) crystal to generate ~ 1 – 2 mJ of pulsed UV radiation at 243nm. The 243nm beam is then sent into the detection chamber. A mirror is mounted behind the photo ionization region to produce counter-propagating beams for the doppler free two photon excitation. The 243 nm photons efficiently ionize the H and the H^+ ions are detected by an MCP. The MCP creates a voltage signal, which is read out by an oscilloscope. In Fig. 6, such a waveform of H^+ signal is shown.

As indicated in Fig. 5, the frequency of the fundamental of the seeder laser is determined and controlled by a wavelength meter.⁴ While the wavelength meter is reliable for relative measurements, the absolute values are shifted by ~ 230 MHz, due to outdated calibration. The CW fundamental frequency corresponds to $1/8$ of the 1S-2S transition frequency, due to two SHG processes and the two photon excitation.

Scanning the laser frequency around the resonance shows that we are capable to resolve the hyperfine splitting (HFS) of H . The two peaks, shown in Fig. 7, correspond to the difference of the HFS of the 1S and the 2S state. The measured value is $\Delta\nu_{\text{meas.}} = 1.23 \pm 0.02$ GHz, which agrees with the literature value $\Delta\nu_{\text{lit.}} = 1.24$ GHz (which can be calculated from [57]) within 1σ . This proves, that we detect H atoms, and not any other potential pollutant in the detection chamber.

A scan of the laser pulse intensity dependency of the signal resulted in the same conclusion, showing the expected behavior. The intensity I is determined by the pulse energy E and the beam waist $\omega_0 \sim 0.75$ mm: $I = E/(\omega_0^2\pi)$.

The data can be taken from Fig. 8.

The signal shows an I^3 dependence as expected for a three photon process. The two photon 1S-2S excita-

⁴ HighFinesse WS7-60.

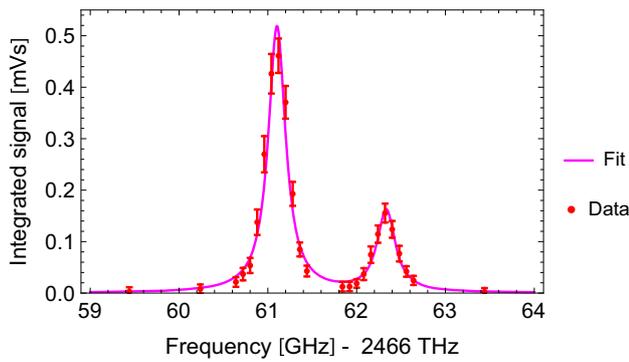


Fig. 7 Laser frequency sweep - Observation of the 1S and 2S HFS of *H*. The frequency values on the abscissa correspond to the measured frequency of the seeder laser fundamental, shifted by 230MHz (outdated wavelength meter calibration) and multiplied by a factor of 8 (two SHG processes, two photon excitation). This was done to match the absolute literature values [57]

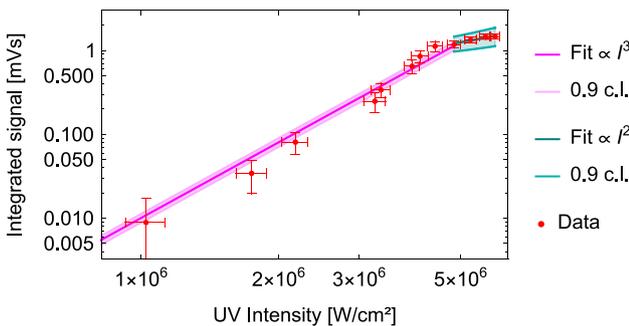


Fig. 8 Laser intensity scan - Observation of the I^3 and I^2 dependency of *H* ionization

tion is I^2 dependent and the ionization of the 2S state adds another I dependency to the overall process. At $\sim 10^7 \text{ W cm}^{-2}$, the 2S ionization process starts to saturate, as the ionization rate $\Gamma_i = (I/h\nu)\sigma$, where σ is the 2S *H* ionization cross section and $h\nu$ the photon energy, reaches $1/\tau_{2S}$, where τ_{2S} is the lifetime of the 2S state. From here, the overall process follows an I^2 dependency. At $\sim 3 \times 10^7 \text{ W cm}^{-2}$, also the 1S-2S excitation process will start to saturate and the overall process becomes I independent [58].

It would be ideal to run the *H* detection on saturation, because the ionization process would become independent of energy- or frequency instabilities of the laser. In order to reach the point of saturation, the laser beam size has to be decreased. Different combinations of convex and concave lenses were already used to compress the beam. But, the mirrors did not withstand the increased intensity for long and were damaged. It seemed like the point of saturation overlapped with the damage threshold of the UV mirrors, which were used at that point. We replaced the mirrors and will hopefully be able to increase the intensity until saturation is reached.

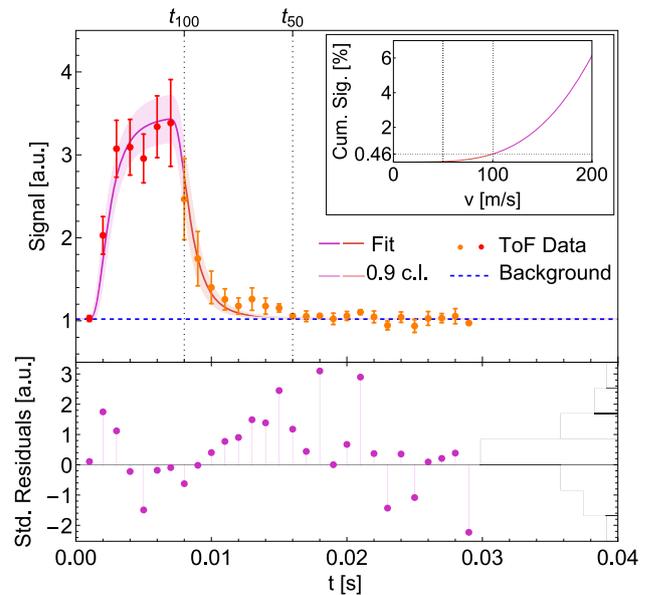


Fig. 9 Upper figure: ToF data and fit. The fit results in a temperature of $T = 6.07 \pm 0.74 \text{ K}$. t_{100} and t_{50} correspond to the ToFs of *H* with velocities of 100 m s^{-1} and 50 m s^{-1} , respectively. In the small figure, the corresponding cumulative velocity distribution for $v \in [0, 200] \text{ m s}^{-1}$ is shown. Lower figure: Standardized residuals of the fit and corresponding histogram

4.2 Hydrogen beam characterization and rate estimation

To characterize the velocity distribution of the *H*-beam, a time of flight (ToF) measurement was performed. The delay between the opening of the chopper and the firing of the laser was varied while the *H* count rate was measured.

The expected signal $S(t)$ is a convolution of the chopper kernel $h(t)$ and the atomic ToF distribution $P_t(t)$ (assumed to follow a Maxwellian distribution) and is given by

$$S(t) = h(t) * P_t(t), \tag{1}$$

$$P_v(t) \propto v^3 \exp\left(-\frac{mv^2}{2kT}\right), \tag{2}$$

$$P_t(t) = P_v\left(\frac{\Delta x}{t}\right) \frac{\Delta x}{t^2}, \tag{3}$$

where Δx is the distance between chopper and detection region, m is the *H* mass, k is the Boltzmann constant and T the temperature.

The data taken in 2021 and a fit are shown in Fig. 9. The fit resulted in a temperature of $T = 6.07 \pm 0.74 \text{ K}$, meaning, that the *H* gas thermalizes well with the cryogenic nozzle at 6K.

The measurement shows that the maximum of the atom flux appears after around 5ms delay, relating to an atomic velocity of 250 m s^{-1} with a significant fraction of atoms below 100 m s^{-1} .

As mentioned in Sect. 3.2, H velocities of up to 100 m s^{-1} can be tolerated. For the upcoming GQS measurement, a certain velocity interval will be selected by setting the delay between chopper opening and firing of the laser to a certain value. The width of this interval is determined by the duration of the chopper opening $t_{\text{open}} \sim 6.1\text{ ms}$. With the current velocity distribution of the H beam, it makes sense, to set the upper bound of the velocity interval to $v_{\text{max}} = 100\text{ m s}^{-1}$ which leads to a lower bound of $v_{\text{min}} = \Delta x / (t_{100} + t_{\text{open}}) = 62\text{ m s}^{-1}$. The mean velocity of this interval is $\bar{v} = 81\text{ m s}^{-1}$ with a corresponding ToF of $t_{\bar{v}} = 12.3\text{ ms}$.

With the fit result, it is possible to estimate the rate of H atoms passing through the future GQS region. It is composed of the H input rate $R_{\text{in}} \sim E17\text{ s}^{-1}$, the chopper duty cycle $d_c \sim 0.061$, the form of the distribution after the chopper, assuming a cone like distribution with an opening angle of $\theta \sim \frac{3}{4}\pi$, the cross-sectional area of the GQS region $A \sim 0.5\text{ mm}^2$ ($\Delta z \sim 20\text{ }\mu\text{m}$, $\Delta y \sim 25\text{ mm}$), the beam waist of the laser $\omega_0 \sim 0.75\text{ mm}$ and the probability of the atoms with the given velocity distribution to have a velocity within the selected velocity interval, $P_v(v_{\text{min}} \geq v_x \geq v_{\text{max}}) = 3.9 \times 10^{-3}$. These parameters yield an estimated rate of H passing through the GQS chamber of

$$R = R_{\text{in}} dP_v(v_{\text{min}} \geq v_x \geq v_{\text{max}}) \frac{A}{2\pi\Delta x^2 (1 - \cos\theta/2)} \frac{2\omega_0}{(v_{\text{max}} - v_{\text{min}})t_{\bar{v}}} \cong 10^4\text{ s}^{-1}. \quad (4)$$

Multiplying R by the ionization efficiency of $\epsilon_{\text{ion}} \sim 8\%$ (determined by ω_0 and an assumed laser energy of 1 mJ) and the MCP efficiency $\epsilon_{\text{MCP}} \sim 50\%$ yields the signal rate $R_{\text{sig}} \cong 400\text{ s}^{-1}$. This is 4×10^3 times more H signal, as compared to the UCN signal.

5 Outlook

There are currently three major improvements being implemented and tested.

New UV mirrors with a higher damage threshold were installed. It can be expected, that the laser intensity will be improved by an order of magnitude: when the beam size is compressed to $\omega_0 \sim 0.3\text{ mm}$, with a UV laser energy of $\sim 1\text{ mJ}$, the intensity becomes $\sim 3.6 \times 10^7\text{ W cm}^{-2}$. At this level, saturation is reached and the signal becomes independent of laser energy- or frequency fluctuations. Furthermore the ionization efficiency will be improved dramatically. A beam size of 0.3 mm yields an ionization efficiency of $\epsilon_{\text{ion}} = 98.22\%$, which would improve the estimated rate by a factor of 12.

The estimated rate will further be improved, by the installation of a new coldhead and an additional heat-shield. This is currently being implemented, and first measurements show, that temperatures around $\sim 4\text{ K}$ can be expected. This would improve our estimated rate

for the velocity interval $[62\text{ m s}^{-1}, 100\text{ m s}^{-1}]$ by a factor of ~ 2.2 . It would alternatively be possible to select slower velocities in the interval $[55\text{ m s}^{-1}, 83\text{ m s}^{-1}]$ while maintaining the same countrate as with the old cryo system.

It would be preferable to go to even lower velocities. But, as shown in Fig. 9 at around 20 ms , the residual hydrogen gas in the chamber prevents the measurements to be sensitive to atoms with lower velocities. This could be improved by an aperture system between the source and the chamber where the GQS region will be installed. Such a system is currently being installed and tested. It consists of three height adjustable, vertical slits with a width of $200\text{ }\mu\text{m}$ for the first slit and 1 mm for the second and third. Two more vacuum pumps will be installed in between the first and the second and the second and the third slit. This system has two purposes: It will decrease the background, due to the separation of the different vacuum regions of the cryogenic chamber, the beamline and the detection chamber. It will also act as a velocity selecting aperture. As the slit height is adjustable, different trajectories of the atoms can be selected. With the three slits, it will be possible to select the low energy tail of the H atoms with a vertical velocity component $v_z \sim 0$ at the entrance of the GQS spectrometer as described in section 3.1.

As soon as those new implementations are completed and characterized, the GQS chamber will be installed at the end of the beamline replacing the detection chamber. It will contain the GQS spectrometer and the viewports for the UV laser. In this way, the atoms passing through the spectrometer will be photo ionized at the end of the mirror and the H^+ detected in the MCP.

6 Conclusions

We conclude that a GQS measurement with H is a very promising but challenging endeavor. The expected count rate exceeds the count rates accessible with UCNS by orders of magnitudes.

An extension and improvement of the existing GQS measurements are highly interesting for multiple fields.

In the course of realizing a GQS measurement with H , we set up a cryogenic H -beam. A highly efficient H detection system was developed. New UV mirrors, an improved cryogenic system and an aperture system which will reduce the background and select ideal velocity components are currently being implemented and tested.

We aim to demonstrate the existence of GQS of H within the next measurement campaign, starting in 2023.

Acknowledgements This project was supported by the Austrian Science Fund (FWF) [W1252-N27] (Doktoratskolleg Particles and Interactions) and the ETH Zurich Career Seed Grant [SEED-17 20-1]. François Nez and Pauline Yzombard acknowledge support from CNRS (IEA 2021-

2022 QRECH). Paolo Crivelli acknowledges the support of the European Research Council (grant 818053-Mu-MASS) and the Swiss National Science Foundation (grant 197346).

Author contributions

All authors contributed to the study conception and design. Material preparation, data collection and analysis were performed by CK, ZB, PB, OH, KS and PY. The first draft of the manuscript was written by CK and all authors commented on previous versions of the manuscript. All authors read and approved the final manuscript.

Funding Information Open access funding provided by Austrian Science Fund (FWF).

Data Availability Statement This manuscript has no associated data or the data will not be deposited. The datasets generated during and/or analyzed during the current study are available from the corresponding author on request.

Open Access This article is licensed under a Creative Commons Attribution 4.0 International License, which permits use, sharing, adaptation, distribution and reproduction in any medium or format, as long as you give appropriate credit to the original author(s) and the source, provide a link to the Creative Commons licence, and indicate if changes were made. The images or other third party material in this article are included in the article's Creative Commons licence, unless indicated otherwise in a credit line to the material. If material is not included in the article's Creative Commons licence and your intended use is not permitted by statutory regulation or exceeds the permitted use, you will need to obtain permission directly from the copyright holder. To view a copy of this licence, visit <http://creativecommons.org/licenses/by/4.0/>.

References

1. G. Breit, The propagation of schroedinger waves in a uniform field of force. *Phys. Rev.* **32**, 273–276 (1928). <https://doi.org/10.1103/PhysRev.32.273>
2. V.I. Luschikov, A.I. Frank, Quantum effects occurring when ultracold neutrons are stored on a plane. *JETP Lett. (USSR) (Engl. Transl.); (United States)* **28:9** (1978). <https://www.osti.gov/biblio/6125370>
3. V. Nesvizhevsky, H. Borner, A. Gagarski, G. Petrov, A. Petukhov, H. Abele, S. Baessler, T. Stoferle, S. Soloviev, Search for quantum states of the neutron in a gravitational field: gravitational levels. *Nucl. Instr. Meth. A* **440**, 754 (2000). [https://doi.org/10.1016/S0168-9002\(99\)01077-3](https://doi.org/10.1016/S0168-9002(99)01077-3)
4. V. Nesvizhevsky, H. Borner, A. Petukhov, H. Abele, S. Baessler, F. Ruess, T. Stoferle, A. Westphal, A. Gagarski, G. Petrov, A. Strelkov, Quantum states of neutrons in the Earth's gravitational field. *Nature* **415**, 297 (2002). <https://doi.org/10.1038/415297a>
5. V. Nesvizhevsky, H. Borner, A. Gagarski, A. Petoukhov, G. Petrov, H. Abele, S. Baessler, G. Divkovic, F. Ruess, T. Stoferle, A. Westphal, A. Strelkov, K. Protasov, A. Voronin, Measurement of quantum states of neutrons in the earth's gravitational field. *Phys. Rev. D* **67**, 102–002 (2003). <https://doi.org/10.1103/PhysRevD.67.102002>
6. V. Nesvizhevsky, A. Petoukhov, H. Borner, K. Protasov, A. Voronin, A. Westphal, S. Baessler, H. Abele, A. Gagarski, Reply to “comment on ‘measurement of quantum states of neutrons in the earth's gravitational field’ “. *Phys. Rev. D* **68**, 108–702 (2003). <https://doi.org/10.1103/PhysRevD.68.108702>
7. V. Nesvizhevsky, A. Petukhov, H. Borner, T. Baranova, A. Gagarski, G. Petrov, K. Protasov, A. Voronin, S. Baessler, H. Abele, A. Westphal, L. Lucovac, Study of the neutron quantum states in the gravity field. *Eur. Phys. J. C* **40**, 479 (2005). <https://doi.org/10.1140/epjc/s2005-02135-y>
8. A. Westphal, H. Abele, S. Baessler, V. Nesvizhevsky, K. Protasov, A. Voronin, A quantum mechanical description of the experiment on the observation of gravitationally bound states. *Eur. Phys. J. C* **51**, 367 (2007). <https://doi.org/10.1140/epjc/s10052-007-0283-x>
9. V. Nesvizhevsky, A. Voronin, R. Cubitt, K. Protasov, Neutron whispering gallery. *Nature Phys.* **6**, 114 (2010)
10. R. Robinett, Quantum wave packet revivals. *Phys. Rep.* **392**, 1 (2004). <https://doi.org/10.1016/j.physrep.2003.11.002>
11. M. Berberan-Santos, E. Bodunov, L. Pogliani, Classical and quantum study of the motion of a particle in a gravitational field. *J. Math. Chem.* **37**, 101 (2005). <https://doi.org/10.1007/s10910-004-1443-y>
12. W. Mather, R. Fox, Coherent-state analysis of the quantum bouncing ball. *Phys. Rev. A* **73**, 032–109 (2006). <https://doi.org/10.1103/PhysRevA.73.032109>
13. O. Bertolami, J. Rosa, Quantum and classical divide: the gravitational case. *Phys. Lett. B* **633**, 111 (2006). <https://doi.org/10.1016/j.physletb.2005.11.041>
14. E. Romera, F. de los Santos, Identifying wave-packet fractional revivals by means of information entropy. *Phys. Rev. Lett.* **99**, 263–601 (2007). <https://doi.org/10.1103/PhysRevLett.99.263601>
15. G.D. Valle, M. Savoini, M. Ornigotti, P. Laporta, V. Foglietti, M. Finazzi, L. Duo, S. Longhi, Experimental observation of a photon bouncing ball. *Phys. Rev. Lett.* **102**, 180–402 (2009). <https://doi.org/10.1103/PhysRevLett.102.180402>
16. I. Garanovich, S. Longhi, A. Sukhorukov, Y. Kivshar, Light propagation and localization in modulated photonic lattices and waveguides. *Phys. Rep.* **518**, 1 (2012). <https://doi.org/10.1016/j.physrep.2012.03.005>
17. M. Belloni, R. Robinett, The infinite well and dirac delta function potentials as pedagogical, mathematical and physical models in quantum mechanics. *Phys. Rep.* **540**, 25 (2014). <https://doi.org/10.1016/j.physrep.2014.02.005>
18. H. Abele, S. Baessler, A. Westphal, (2003), p. 355
19. A. Frank, P.V. Isacker, J. Gomez-Camacho, Probing additional dimensions in the universe with neutron experiments. *Phys. Lett. B* **582**, 15 (2004). <https://doi.org/10.1016/j.physletb.2003.12.026>

20. F. Brau, F. Buisseret, Minimal length uncertainty relation and gravitational quantum well. *Phys. Rev D* **74**(3) (2006). <https://doi.org/10.1103/physrevd.74.036002>
21. F. Buisseret, B. Silvestre-Brac, V. Mathieu, Modified newton's law, braneworlds and the gravitational quantum well. *Class. Quant. Grav.* **24**, 855 (2007). <https://doi.org/10.1088/0264-9381/24/4/006>
22. S. Baessler, V. Nesvizhevsky, K. Protasov, A. Voronin, Constraint on the coupling of axionlike particles to matter via an ultracold neutron gravitational experiment. *Phys. Rev. D* **75**, 075–006 (2007). <https://doi.org/10.1103/PhysRevD.75.075006>
23. I. Antoniadis, S. Baessler, M. Buechner, V. Fedorov, S. Hoedl, A. Lambrecht, V. Nesvizhevsky, G. Pignol, K. Protasov, S. Reynaud, Y. Sobolev, Short-range fundamental forces. *Compt. Rend. Phys.* **12**, 755 (2011). <https://doi.org/10.1016/j.crhy.2011.05.004>
24. P. Brax, G. Pignol, Strongly coupled chameleons and the neutronic quantum bouncer. *Phys. Rev. Lett.* (2011). <https://doi.org/10.1103/PhysRevLett.107.111301>
25. O. Bertolami, F. Nunes, Ultracold neutrons, quantum effects of gravity and the weak equivalence principle. *Class. Quant. Grav.* **20**, L61 (2003). <https://doi.org/10.1088/0264-9381/20/5/103>
26. C. Kiefer, C. Weber, On the interaction of mesoscopic quantum systems with gravity. *Ann. Phys.* **14**, 253 (2005). <https://doi.org/10.1002/andp.200410119>
27. E. Kajari, N. Harshman, E. Rasel, S. Stenholm, G. Suessmann, W. Schleich, Inertial and gravitational mass in quantum mechanics. *Appl. Phys. B* **100**, 43 (2010). <https://doi.org/10.1007/s00340-010-4085-8>
28. O. Bertolami, J. Rosa, C. de Aragao, P. Castorina, D. Zappala, Noncommutative gravitational quantum well. *Phys. Rev. D* (2005). <https://doi.org/10.1103/PhysRevD.72.025010>
29. A. Saha, Time-space non-commutativity in gravitational quantum well scenario. *Europ. Phys. J. C* **51**, 199 (2007). <https://doi.org/10.1140/epjc/s10052-007-0274-y>
30. K. Nozari, P. Pedram, Minimal length and bouncing-particle spectrum. *EPL* (2010). <https://doi.org/10.1209/0295-5075/92/50013>
31. P. Pedram, K. Nozari, S. Taheri, The effects of minimal length and maximal momentum on the transition rate of ultra cold neutrons in gravitational field. *J. High En. Phys.* (2011). [https://doi.org/10.1007/JHEP03\(2011\)093](https://doi.org/10.1007/JHEP03(2011)093)
32. A. Kobakhidze, Gravity is not an entropic force. *Phys. Rev. D* (2011). <https://doi.org/10.1103/PhysRevD.83.021502>
33. M. Chaichian, M. Oksanen, A. Tureanu, On gravity as an entropic force. *Phys. Lett. B* **702**, 419 (2011). <https://doi.org/10.1016/j.physletb.2011.07.019>
34. A. Martin-Ruiz, C. Escobar, Testing lorentz and cpt invariance with ultracold neutrons. *Phys. Rev. D* (2018). <https://doi.org/10.1103/PhysRevD.97.095039>
35. C. Escobar, A. Martin-Ruiz, Gravitational searches for lorentz violation with ultracold neutrons. *Phys. Rev. D* (2019). <https://doi.org/10.1103/PhysRevD.99.075032>
36. A. Ivanov, M. Wellenzohn, H. Abele, Probing of violation of lorentz invariance by ultracold neutrons in the standard model extension. *Phys. Lett. B* (2019). <https://doi.org/10.1016/j.physletb.2019.134819>
37. V. Nesvizhevsky, K. Protasov, in: *Trends in Quantum Gravity Research*, Editor: David C. Moore, pp. 65-107 (2006)
38. V. Nesvizhevsky, Near-surface quantum states of neutrons in the gravitational and centrifugal potentials. *Phys. Usp.* **53**, 645 (2010). <https://doi.org/10.3367/UFNe.0180.201007a.0673>
39. T. Jenke, P. Geltenbort, H. Lemmel, H. Abele, Realization of a gravity-resonance-spectroscopy technique. *Nat. Phys.* **7**, 468 (2011). <https://doi.org/10.1038/NPHYS1970>
40. T. Jenke, G. Cronenberg, J. Burgdoerfer, L. Chizhova, P. Geltenbort, A. Ivanov, T. Lauer, T. Lins, S. Rotter, H. Saul, U. Schmidt, H. Abele, Gravity resonance spectroscopy constrains dark energy and dark matter scenarios. *Phys. Rev. Lett.* (2014). <https://doi.org/10.1103/PhysRevLett.112.151105>
41. G. Ichikawa, S. Komamiya, Y. Kamiya, Y. Minami, M. Tani, P. Geltenbort, K. Yamamura, M. Nagano, T. Sanuki, S. Kawasaki, M. Hino, M. Kitaguchi, Observation of the spatial distribution of gravitationally bound quantum states of ultracold neutrons and its derivation using the wigner function. *Phys. Rev. Lett.* (2014). <https://doi.org/10.1103/PhysRevLett.112.071101>
42. A. Voronin, P. Froelich, V. Nesvizhevsky, Gravitational quantum states of antihydrogen. *Phys. Rev. A* **83**, 032–903 (2011). <https://doi.org/10.1103/PhysRevA.83.032903>
43. P.P. Crepin, G. Dufour, R. Guerout, A. Lambrecht, S. Reynaud, Casimir-polder shifts on quantum levitation states. *Phys. Rev. A* (2017). <https://doi.org/10.1103/PhysRevA.95.032501>
44. G. Dufour, A. Gerardin, R. Guerout, A. Lambrecht, V.V. Nesvizhevsky, S. Reynaud, A.Y. Voronin, Quantum reflection of antihydrogen from the casimir potential above matter slabs. *Phys. Rev. A* (2013). <https://doi.org/10.1103/PhysRevA.87.012901>
45. T. Pasquini, Y. Shin, C. Sanner, M. Saba, A. Schirotzek, D. Pritchard, W. Ketterle, Quantum reflection from a solid surface at normal incidence. *Phys. Rev. Lett.* (2004). <https://doi.org/10.1103/PhysRevLett.93.223201>
46. V. Druzhinina, M. DeKieviet, Experimental observation of quantum reflection far from threshold. *Phys. Rev. Lett.* (2003). <https://doi.org/10.1103/PhysRevLett.91.193202>
47. I. Yu, J. Doyle, J. Sandberg, C. Cesar, D. Kleppner, T. Greytak, Evidence for universal quantum reflection of hydrogen from liquid-he-4. *Phys. Rev. Lett.* **71**(10), 1589–1592 (1993). <https://doi.org/10.1103/PhysRevLett.71.1589>
48. J. Berkhout, O. Luiten, I. Setija, T. Hijmans, T. Mizusaki, J. Walraven, Quantum reflection-focusing of hydrogen-atoms with a concave mirror. *Phys. Rev. Lett.* **63**(16), 1689–1692 (1989). <https://doi.org/10.1103/PhysRevLett.63.1689>
49. M. Berry, K. Mount, Semiclassical approximations in wave mechanics. *Rep. on prog. Phys.* **35**(4), 315 (1972). <https://doi.org/10.1088/0034-4885/35/1/306>
50. H. Friedrich, J. Trost, Working with wkb waves far from the semiclassical limit. *Phys. Rep. Rev. Sect. Phys.*

- Lett. **397**(6), 359–449 (2004). <https://doi.org/10.1016/j.physrep.2004.04.001>
51. S.F. Cooper, A.D. Brandt, C. Rasor, Z. Burkley, D.C. Yost, Cryogenic atomic hydrogen beam apparatus with velocity characterization. *Rev. Sci. Instrum.* **91**(1), 013–201 (2020)
 52. R. Golub, D. Richardson, S. Lamoreaux, *Ultra-Cold Neutrons* (Taylor & Francis, 1991). <https://books.google.at/books?id=QPUjlcWNg78C>
 53. M. Diermaier, C. Jepsen, B. Kolbinger, C. Malbrunot, O. Massiczek, C. Sauerzopf, M. Simon, J. Zmeskal, E. Widmann, In-beam measurement of the hydrogen hyperfine splitting and prospects for antihydrogen spectroscopy. *Nature Commun.* (2017). <https://doi.org/10.1038/ncomms15749>
 54. P. Crivelli, The mu-mass (muonium laser spectroscopy) experiment. *Hyperfine Interact.* **239**(1), 49 (2018)
 55. B. Ohayon, G. Janka, I. Cortinovis, Z. Burkley, L.d.S. Borges, E. Depero, A. Golovizin, X. Ni, Z. Salman, A. Suter, C. Vigo, T. Prokscha, P. Crivelli, Precision measurement of the lamb shift in muonium. *Phys. Rev. Lett.* **128**, 011-802 (2022). <https://doi.org/10.1103/PhysRevLett.128.011802>
 56. P. Pérez et al., The GBAR antimatter gravity experiment. *Hyperfine Interact.* **233**(1–3), 21–27 (2015). <https://doi.org/10.1007/s10751-015-1154-8>
 57. C.G. Parthey, et al., Improved Measurement of the Hydrogen 1S - 2S Transition Frequency. *Phys. Rev. Lett.* **107**, 203-001 (2011). <https://doi.org/10.1103/PhysRevLett.107.203001>. [arXiv:1107.3101](https://arxiv.org/abs/1107.3101) [physics.atom-ph]
 58. S.W. Downey, R.S. Hozack, Saturation of three-photon ionization of atomic hydrogen and deuterium at 243 nm. *Opt. Lett.* **14**(1), 15–17 (1989). <https://doi.org/10.1364/OL.14.000015>. <https://opg.optica.org/ol/abstract.cfm?URI=ol-14-1-15>